ACS OMEGA

http://pubs.acs.org/journal/acsodf

Article

Catalytic and Medical Potential of a Phyto-Functionalized Reduced Graphene Oxide−Gold Nanocomposite Using Willow-Leaved Knotgrass

Nourhan El-Maghrabi, Ola M. El-Borady, Mohamed Hosny,* and Manal Fawzy

Cite This: *ACS Omega* 2021, 6, 34954−34966

Read Online

ACCESS | Metrics & More | Article Recommendations | Supporting Information

ABSTRACT: In the current study, a simple, environmentally friendly, and cost-effective reduced graphene oxide−gold nanoparticle (rGO-AuNP) nanocomposite was successfully phytosynthesized using the aqueous leaf extract of a common weed found on the Nile banks, *Persicaria salicifolia*, for the first time. The phytosynthesis of rGO-AuNPs was first confirmed *via* the color transformation from brown to black as well as throughvarious techniques such as transmission electron microscopy (TEM) and Raman spectroscopy. Two UV−vis peaks at 275 and 530 nm were observed for the nanocomposite with a typical particle size of mostly spherical AuNPs of 15−20 nm. However, other shapes were occasionally detected including rods, triangles, and rhomboids. Existing phytoconstituents such as flavonoids and glycosides in the plant extract were suggested to be responsible for the phytosynthesis of rGO-AuNPs. The excellent catalytic efficacy of rGO-AuNPs against MB degradation was confirmed, and a high antibacterial efficiency against *Escherichia coli* and *Klebsiella pneumonia* was also confirmed. Promising antioxidant performance of rGO-AuNPs was also proved. Furthermore, it was concluded that rGO-AuNPs acquired higher efficiency than AuNPs synthesized from the same plant extract in all of the studied applications.

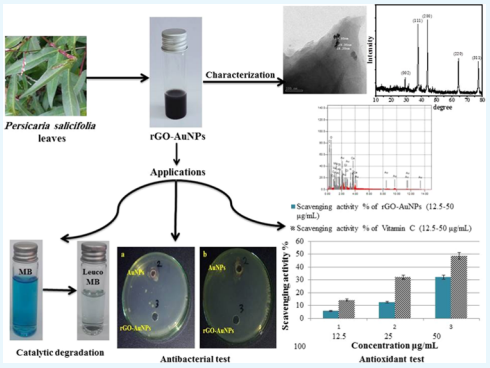

1. INTRODUCTION

Nanomaterials have been dramatically scrutinized and utilized in numerous applications in recent years based on their outstanding properties.[1−3] Quantum dots, nanotubes, nanofibers, nanowires, and nanomembranes are the most well-known types of nanomaterials adopted in various applications.[4,5] The extremely small size and large surface area of nanomaterials endow them with completely different chemical and physical properties than their bulky counterparts with macrosize.[6,7]

A fascinating carbon nanomaterial that possesses very unique and unusual characteristics is graphene. The graphene structure is considered to be the basic structure of all carbon nanomaterials as it is a sheet of sp^2-bonded carbon atoms with a thickness of only one atom arranged in the form of a hexagonal pattern.[8,9] Graphene exhibits several outstanding characteristics including an extraordinary carrier mobility of up to 200 000 cm^2 $(V\ s)^{-1}$, a large specific surface area that can reach 2630 m^2 g^{-1}, and a transmittance of 97.7%.[10,11] Generally, 2D materials such as graphene have great potential for high-performance photodetectors due to their high crystal quality and unique properties in both electronic and optical aspects such as tunable bandgaps with thickness variations.[12] Moreover, adding inorganic metallic nanoparticles can help in stabilizing the produced graphene and in preventing its aggregation because the presence of these nanoparticles results in increasing the interlayer distance of graphene layers, which makes the two faces available for a reaction.[13,14]

Gold nanoparticles (AuNPs) have high reactivity and can be attached to molecules of biological relevance. Based on the irreversible self-agglomeration, colloidal instability, poor reliability, and nonspecificity of graphene, it is not suitable for use in its sole form in many applications.[15] These limitations could be overcome by adding AuNPs to graphene, which results in a hybrid nanocomposite with increased surface area, catalytic activity, solubility, and biocompatibility.[16] Graphene−gold nanocomposites (rGO-AuNPs) can act synergistically to offer several unique physicochemical properties. rGO-AuNPs have attracted the interest of most researchers because of their significantly enhanced sensitivity and selectivity. Thus, they can be harnessed in the degradation of toxic organic pollutants compared to bare graphene or AuNPs.[17]

Lithography, laser ablation, and pyrolysis are the common techniques used to synthesize graphene.[18,19] In general, these

Received: October 7, 2021
Accepted: November 24, 2021
Published: December 8, 2021

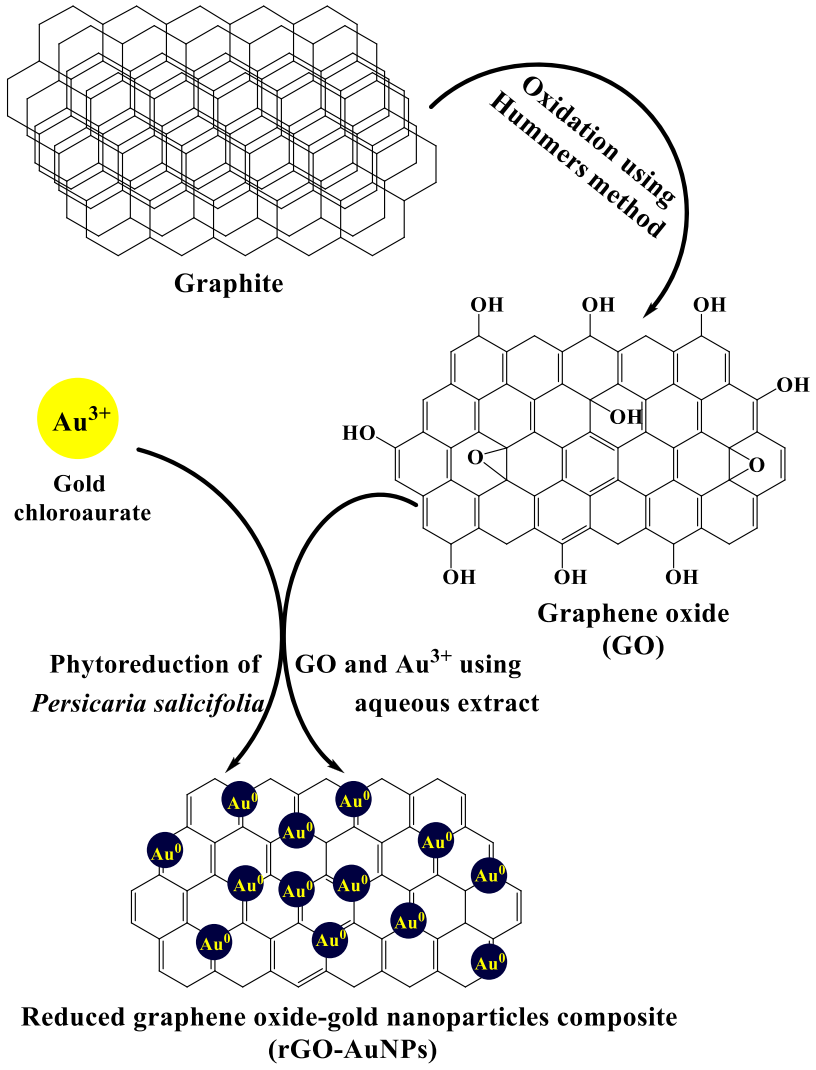

Figure 1. Proposed mechanism for the phytosynthesis of the rGO-AuNP nanocomposite using the *P. salicifolia* extract.

techniques are expensive and perilous as they often involve toxic reducing agents and harsh reaction conditions[20,21] for the sake of high yield production. Plants and other organisms can sustainably produce nanomaterials in a green, safe, and cost-effective way.[20,22] Microorganisms are not deemed to be the best option as they often require careful handling and maintenance, which adds to the cost.[23,24] Synthesis of nanoparticles is deemed to be faster, easier, and more suitable when using plant-derived extracts as they contain a variety of phytoconstituents that simultaneously serve as reducing and capping agents, resulting in diminished synthesis costs and the production of environmentally friendly nanomaterials.[25,26]

Textile manufacturing is among the major sources that pose perilous ecological threats to the surrounding environments, particularly aquatic ecosystems. Untreated wastewater from the textile industry containes toxic organic dyes such as methylene blue (MB).[27,28] The application of nanomaterials including PtNPs, AgNPs, and AuNPs as antimicrobial agents is well documented. Among the pathogenic bacterial strains, *Staphylococcus aureus* and *Escherichia coli*[29] cause urinary tract infections, enterocolitis, bloodstream infections, pneumonia, and bone infections.[30−32] These bacteria were treated with a variety of antibiotics, but the constant use of these antibiotics led to the evolution of drug-resistant strains of bacteria.[33] Therefore, the pursuit of new effective remedies is considered a priority. Naturally occurring chemicals called antioxidants safeguard cells and tissues from free radical damage.[34] The human body, in general, has a well-developed antioxidant defense mechanism. However, this system sometimes fails to work efficiently under certain conditions. Consequently, exogenous antioxidants are used in these conditions. Among these antioxidants, several metallic nanoparticles (e.g., AuNPs, AgNPs, and PtNPs)[35,36] and also nanocomposites (e.g., rGO-AuNPs) have been confirmed to have a good antioxidant efficiency.[37]

The current study was intended to examine, for the first time, the applicability of synthesizing a rGO-AuNP nanocomposite using the aqueous extract of a common wild plant species found on the Nile banks *Persicaria salicifolia* (*Pluchea salicifolia*), which is commonly known as Willow-Leaved Knotgrass and has never been employed for synthesizing graphene or any other carbon nanomaterial. In addition, a comparison between the performances of rGO-AuNPs and AuNPs, synthesized from the same plant extract, was also made based on their catalytic MB degradation, antibacterial, and antioxidant efficiencies.

https://doi.org/10.1021/acsomega.1c05596
ACS Omega 2021, 6, 34954−34966

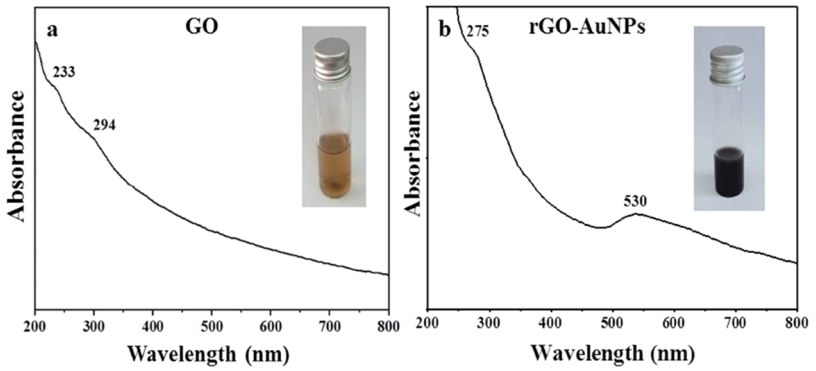

Figure 2. UV−Vis spectra of (a) GO (inset: image of GO solution) and (b) rGO-AuNPs (inset: image of the rGO-AuNP solution).

2. RESULTS AND DISCUSSION

A simplified mechanism for the green synthesis of the rGO-AuNP nanocomposite using the *P. salicifolia* extract is shown in Figure 1 according to which the simultaneous reduction of GO, which was obtained after the oxidation of graphite via the Hummers method, and Au^{3+} into the rGO-AuNP nanocomposite was achieved through the active contribution of phytoconstituents including flavonoids, alkaloids, tannins, and other constituents that acted as a reducing and capping agent at the same time obviating the use of chemical reducing agents; these phytoconstituents were verified to be existent in the *P. salicifolia* extract by Youssef and El-Swaify[38] and Salem et al.[39] In addition, these phytoconstituents were proven to be capable of donating electrons or hydrogen atoms to gold ions to get these ions reduced on the surface of the rGO.[40] These studies indicated the high efficacy of employing the aqueous extract of *P. salicifolia* in the biosynthesis of numerous metallic and nonmetallic nanomaterials, mainly *P. salicifolia* exposed to harsh environmental conditions like droughts and high salt concentrations as it has been proven that the concentration of phytoconstituents increases in most living plant species when the harshness of these environmental conditions increases.[41] Furthermore, it has to be mentioned that when AuNPs are synthesized on the surface of rGO sheets, they act as a spacer and prevent the aggregation and restacking of rGO sheets.[42] Subsequently, this resulted in high efficiency of the rGO-AuNP nanocomposite in various tested applications in the current study.

2.1. UV−Visible Spectroscopy. The UV spectrum of GO (Figure 2a) shows two peaks with an obvious absorbance; the first peak at 233 nm due to the $\pi-\pi^*$ transitions of the aromatic C═C bonds and a shoulder peak at 294 nm accredited to then-π^* transitions of the C═O bonds.[43] After GO reduction by the plant extract, a red shift occurred and a new peak at 275 nm was formed while the peak at 294 nm disappeared and another peak was observed at 530 nm as shown in Figure 2b, which was accredited to the surface plasmon resonance (SPR) of AuNPs, indicating the successful phytosynthesis of rGO-AuNPs. Therefore, it was confirmed that the phytoconstituents of the plant extract could act as an effective reducing and capping agent. In line with the obtained results, Tabrizi and Varkani[44] used rose water extract for the preparation of rGO-AuNPs and reported two peaks; at 530 nm confirming the AuNP formation and at 263 nm confirming the reduction of GO. Likewise, Amarnath et al.[45] recorded a peak for AuNPs at 536 nm and a characteristic peak of graphene at 265 nm when *Xanthium strumarium* extract was employed for rGO-AuNP synthesis.

The color transformation of the GO solution from brown (inset of Figure 2a) to black (inset of Figure 2b) further confirmed the successful reduction of GO into rGO-AuNPs and could be mainly accredited to the loss of oxygen-containing moieties as indicated by Maddinedi et al.[46] Such a color change was also detected by Lee and Kim[47] due to the decrease in polar functionality on the surface of the sheets leading to an increase in the hydrophobicity of rGO-AuNPs.

2.2. FTIR Spectroscopy. The functional groups of the extract involved in the reduction and capping of the phytosynthesized rGO-AuNPs were identified using FTIR analysis (Figure 3). Several peaks of oxygen-containing groups

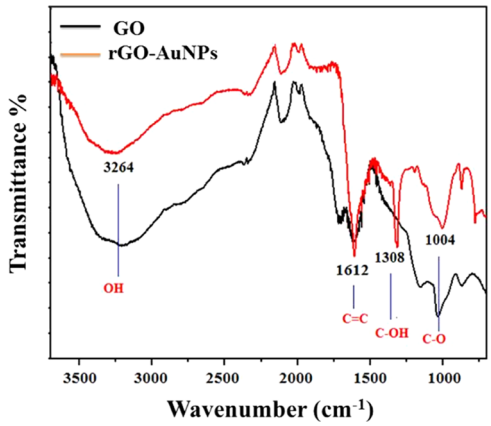

Figure 3. FTIR spectra patterns of GO and rGO-AuNP nanocomposite.

were detected in the FTIR spectrum of GO, indicating the successful oxidation of natural graphite into GO by the modified Hummers method including an O−H group that appeared at 3264 cm^{-1}. The presence of polar groups, especially the O−H group, enables the GO to easily form hydrogen bonds with water molecules and exhibit good hydrophilic properties as elaborated by Li et al.[48] Other functional groups were detected in the GO spectrum, including C═C at 1612 cm^{-1} and C−O at 1004 cm^{-1}.

The FTIR spectra of rGO-AuNPs showed a remarkable diminution in the peak intensity of the oxygen-containing functional groups including the O−H and C−O bands that appeared almost at the same wavenumbers as observed in the case of GO. Thus, the phytoreduction of GO and the formation of the rGO-AuNP nanocomposite were confirmed.

https://doi.org/10.1021/acsomega.1c05596
ACS Omega 2021, 6, 34954−34966

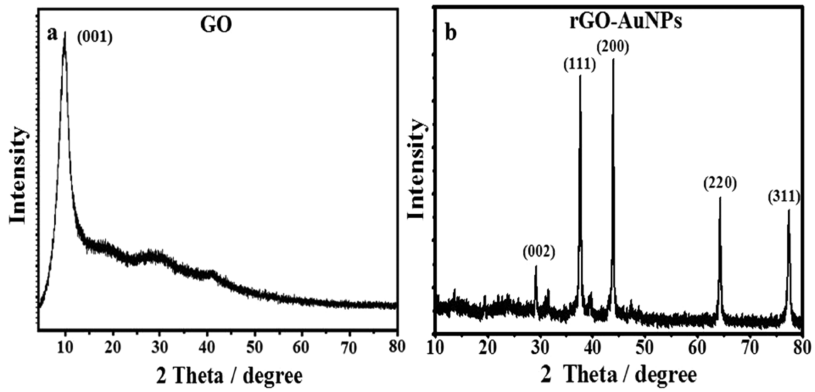

Figure 4. XRD patterns of (a) GO and (b) the rGO-AuNP nanocomposite.

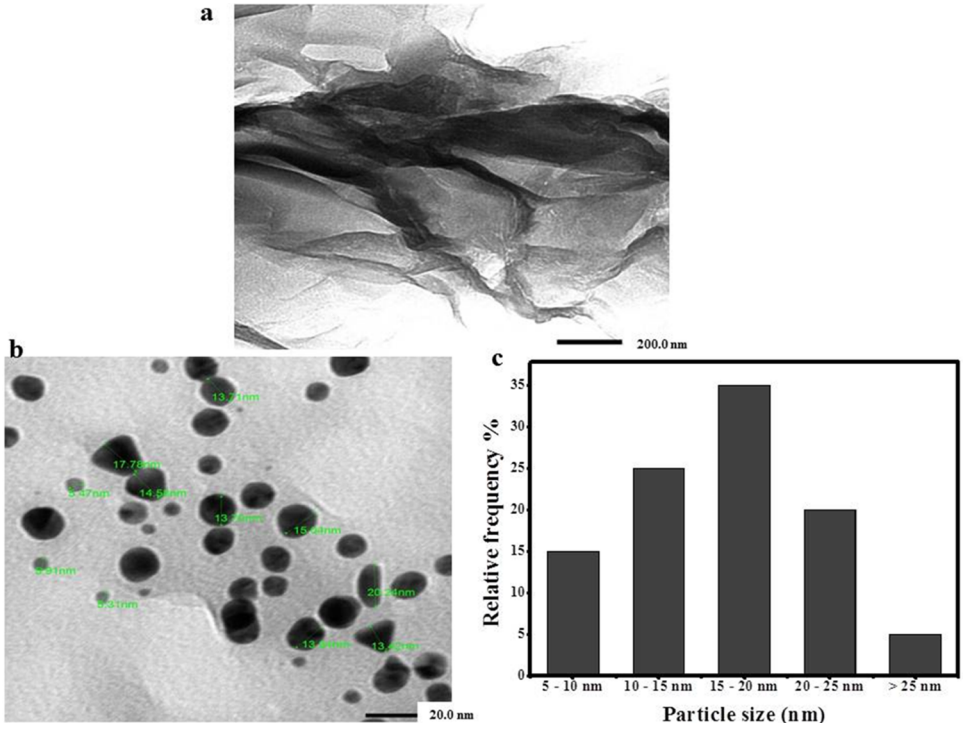

Figure 5. TEM images of (a) multilayered sheets of GO stacked on each other, (b) spherical AuNPs attached to its surface, and (c) histogram of the particle size of rGO-AuNPs.

The appearance of a new C−OH band was accredited to the plant extract moieties. The obtained results could be interpreted by the presence of water-soluble phytoconstituents such as flavonoids, glycosides, and phenolic acids of the *P. salicifolia* aqueous extract, which were previously detected by El-Anwar et al.[49] and Hussein et al.[50] They are responsible for the bioreduction and stabilization of the synthesized graphene together with Au nanoparticles that are decorating its surface.

The obtained results were concomitant with those obtained by Lee and Kim[47] and Mahata et al.[51] who detected that the intensities of oxygen-containing functional groups were considerably reduced when using *Prunus serrulata* and *Ocimum sanctum* extracts, respectively, in GO reduction and similar to those obtained by Khan et al.[52] who observed the presence of additional bands in the FTIR spectrum of rGO synthesized from the extract of *Salvadora persica* and attributed to them to phytomolecules bound to the rGO surface.

2.3. X-ray Diffraction (XRD) Spectroscopy. XRD analysis is generally postulated to be a quintessential tool in providing information about the crystal structure of nanomaterials.[53,54] The XRD pattern of GO (Figure 4a) has a wide diffraction peak at $2\theta = 11.6°$ consistent with the reflection of 001, indicating the successful oxidation of graphite into GO, as was previously elaborated by Mhamane et al.,[55] while the pattern of rGO-AuNPs displayed in Figure 4b confirms the structural changes resulting from the phytosynthesis of the rGO-AuNP nanocomposite. It showed the characteristic peak of graphene at $2\theta = 28.6°$, and the AuNP peaks at 38.2, 44.3, 64.8, and 78.2° were indexed to (111), (200), (220), and (311), which well matched with the JCPDS file number 04-0784 and were in agreement with XRD results reported for green synthesized rGO-AuNPs by many workers.

The strong diffraction pattern of GO indicates the presence of multilayer graphene and oxygen-containing groups, which is normal before the reduction process.[56] However, rGO-AuNP sheets exhibit distinct peaks that seem to be very broad with a lower intensity due to the reduction of GO to rGO by utilizing the plant extract as a reducing agent.[57]

https://doi.org/10.1021/acsomega.1c05596
ACS Omega 2021, 6, 34954−34966

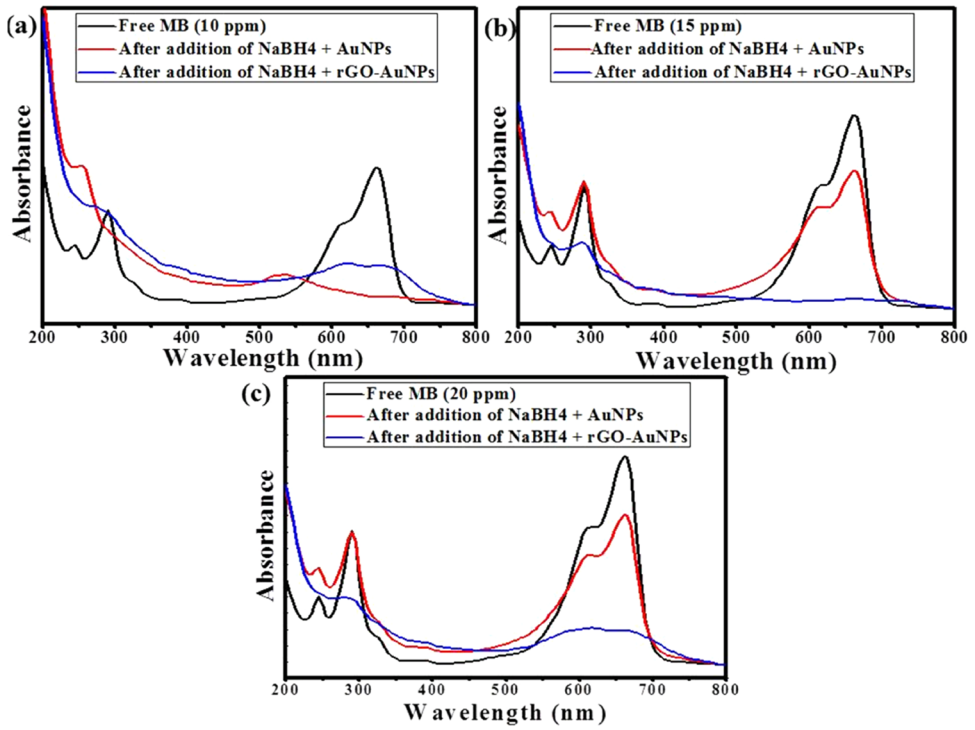

Figure 6. Catalytic degradation of MB solutions with different concentrations of (a) 10 ppm, (b) 15 ppm, and (c) 20 ppm using 0.1 mL of AuNPs + 0.1 mL of $NaBH_4$, and 0.1 mL of rGO-AuNPs + 0.1 mL of $NaBH_4$.

2.4. Transmission Electron Microscopy (TEM). TEM images of GO (Figure 5a) showed obvious dark areas of lamellar folds and stacks. These dark areas indicated the thick stacked nanostructure of several graphene oxide layers with oxygen functional groups,[58] while the TEM image of rGO-AuNPs (Figure 5b) showed a slightly wrinkled, transparent, thin, and few-layered sheet morphology. The slight wrinkles along the edge region could be accredited to the association of rGO with the attached biomolecules as concluded by Jin et al.[59] In addition, these wrinkles were previously stated to be accountable for the thermodynamic stability of two-dimensional graphene.[47]

The distribution of spherical AuNPs with size ranging from 5.49 to 26.58 nm on the surface of rGO sheets was obvious in Figure 5c. Other shapes for AuNPs such as triangles, rods, and rhomboids were also detected. Moreover, a size histogram (Figure 5d) indicated that the size of the majority of AuNPs decorating the rGO surface was in the range from 15 to 20 nm. Our results were in agreement with other phyto-[60,61] and chemosynthesized rGO-AuNP nanocomposites.[62]

2.5. ζ Potential Measurement. ζ potential analysis of GO showed a potential of −30.4 mV as displayed in Figure S1a due to the presence of various oxygen functional groups on its surface.[63] Afterward, it changed to a slightly higher ζ potential of −31.4 mV in rGO-AuNPs (Figure S1b), indicating that the phytosynthesized nanocomposite has more stability than GO. Additionally, the presence of oxidized polyphenols on the surface of rGO-AuNPs after reduction was confirmed. These oxidized polyphenols resulted in higher stability by preventing the agglomeration of rGO-AuNP sheets. These findings were concomitant with those of many workers.[64,65]

2.6. EDX Spectroscopy. Strong signals of gold atoms were detected at several energy levels mostly at 2.2 keV and 1.8, 2.3, 2.8, 4.2, 8.5, 9.8, 11.5, 11.6, and 13.4 keV as presented in Figure S2. Signals for other elements including carbon, oxygen, sodium, potassium, magnesium, and calcium were also detected and suggested to be of plant origin. Moreover, a signal for copper was also detected that could have originated from the carbon-coated copper grid used for analysis, in line with other research works.[61]

2.7. Raman Spectroscopy. Raman spectroscopy is a quintessential tool to examine the ordered−disordered crystal structures of carbonaceous materials, especially for graphene, and it is also an effective means for determining the flake thickness of graphene materials.[66] The obtained results from the spectrum of GO (Figure S3) demonstrated two intense bands at 1352 and 1597 cm^{-1}, corresponding to the D and G bands, respectively. After the reduction of GO to rGO-AuNPs by the plant extract, the D band shifted to 1345.5 cm^{-1}, confirming the formation of few-layered graphene as elaborated by Wang et al.[67] Concerning the G band, it shifted from 1597 to 1587 cm^{-1}, indicating a higher degree of order for rGO-AuNPs owing to the removal of the majority of oxygen-containing functional groups as previously interpreted.[46,68]

The intensity of the G band could be harnessed in determining the number of graphene layers since the number of graphene layers decreases when there is a linear diminution in the G band intensity. Thus, the diminution in G band intensity observed after the GO reduction in the current work indicated a decrease in the number of graphene layers.[69] The intensity ratio between the D and G peaks (I_D/I_G) is utilized to reflect the degree of graphitization of carbonaceous materials, and it shows how effective the reduction process is, being more effective when the intensity ratio is $\lesssim$1.[70] Accordingly, the intensity ratio of the D band relative to the G band could be utilized as an indicator of the structural disorder in the basal plane and the quality of the produced graphene. In this study, the I_D/I_G ratio of rGO-AuNPs was 0.61, which was in line with that reported by Mhamane et al.[55] and less than the defect

https://doi.org/10.1021/acsomega.1c05596
ACS Omega 2021, 6, 34954−34966

Table 1. Comparison between the Catalytic Degradation Efficiency of AuNPs, rGO-AuNPs, and Other Nanocatalysts Reported in Other Studies against MB

catalyst	dye concentration (ppm)	pH	degradation efficiency (%)	time (min)	refs
reduced graphene oxide−gold nanohybrid	10	6	98	10	76
Au-Fe_3O_4/graphene	20	7	99	120	77
reduced graphene oxide magnetic composite (rGO/$CoFe_2O_4$)	20	3	100	24	72
Au-Cu_2O/rGO	20	10.5	99.8	20	78
reduced graphene oxide/meso-TiO_2/AuNPs	30	6	≃100	240	79
manganese-reduced (Mn/RGO) nanocomposite	50		70.4	30	80
manganese-cobalt-reduced (Mn-Co/RGO) nanocomposite			≃100		
reduced graphene oxide−silver (rGO-Ag) nanocomposite			71.42	8	81
rGO-stabilized MnO/N-doped carbon nanofibers	20		100	180	73
MoS_2	200	9	98	30	82
(MoS_2-rGO) nanocomposite				10	
graphene/MnO_2 hybrids	50	6	≃100	5	83
gold nanoparticles (AuNPs)	10	5	≃100	immediately	the current work
	15		26.7		
	20		24		
reduced graphene oxide−gold nanoparticles (rGO-AuNPs)	10		≃100		
	15				
	20				

ratio (I_D/I_G = 1.31) reported by Chabot et al.[71] for chemically synthesized rGO, thus indicating that the rGO-AuNP nanocomposite synthesized by the plant extract acquired high quality and fewer defects than the chemically synthesized graphene.

2.8. Catalytic Degradation of MB. In the current study, the catalytic degradation of different concentrations (10, 15, and 20 ppm) of MB was carried out using only 0.1 mL of green synthesized AuNPs and rGO-AuNP separately in the presence of 0.1 mL of 0.058 M $NaBH_4$. The obtained results indicated the immediate disappearance of the characteristic blue color of MB after the addition of rGO-AuNPs with all of the above-mentioned concentrations as displayed in Figure 6a−c. However, in the case of AuNP addition, the MB color was immediately removed only in the case of the lowest concentration (10 ppm) as shown in Figure 6a. Regarding the higher concentrations, the degradation efficiency was 26.7 and 24% in the case of 15 and 20 ppm, respectively (Figure 6b,c). When control experiments were carried out in the absence of AuNPs or rGO-AuNPs, there was no observed color change. Additionally, when the catalytic degradation efficiency of the *P. salicifolia* extract was examined, it was concluded that the removal efficacy of MB was only 8% as shown in Figure S4, denoting the essential role of the green synthesized AuNPs and rGO-AuNPs in the degradation of MB. Regarding the reusability of rGO-AuNPs, five cycles of reuse were carried out in the removal of MB with a concentration of 15 ppm, and the results showed that the catalytic efficiency remained 100% after two cycles of recycling. Nonetheless, the efficiency began to decrease to 93, 86, and 81% in the third, fourth, and fifth cycles, respectively (Figure S5a,b), confirming the high applicability of rGO-AuNPs as a catalyst.

When the current results were compared to other studies such as those of Wu et al.[72] and Chen et al.[73] who obtained a catalytic degradation efficiency of 100% against MB solutions with the same concentration (20 ppm) used in this study, it was found that they achieved these results within 24 and 180 min, respectively. Therefore, it was concluded that the rGO-AuNP nanocomposite in this work has higher efficiency and faster degradation than other rGO nanocomposites. Consequently, it is considered to be an acceptable catalyst that could be employed in the degradation of MB and other toxic organic pollutants in wastewater. Furthermore, a thorough comparison between AuNPs, rGO-AuNPs, and other nanocatalysts elucidating different variables such as the dye concentration, degradation time, and efficacy is elaborated in Table 1.

A mechanism that clarifies the active role of the rGO-AuNP nanocomposite in the catalytic degradation of MB into leuco MB is displayed in Figure 7 in which rGO-AuNPs have

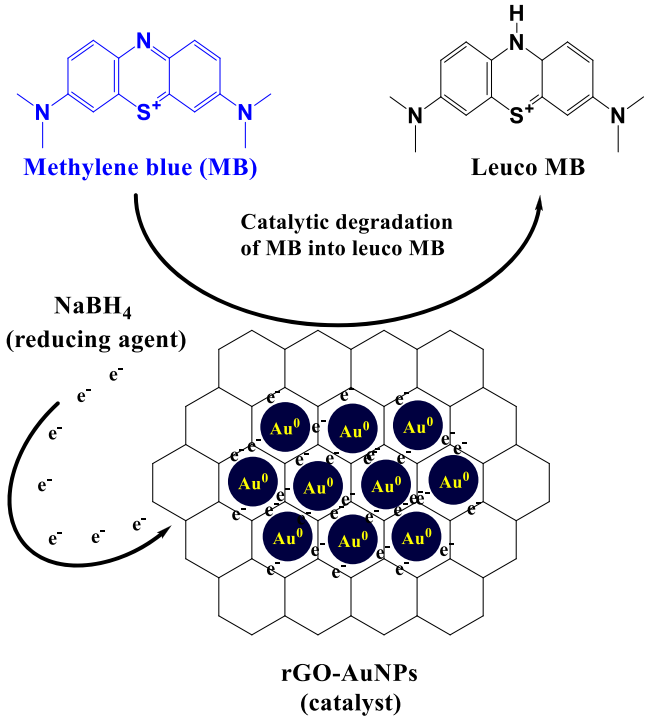

Figure 7. Proposed mechanism for the catalytic degradation of MB using the rGO-AuNP nanocomposite.

https://doi.org/10.1021/acsomega.1c05596
ACS Omega 2021, 6, 34954−34966

effectively transferred the electrons from $NaBH_4$ (reducing agent) into MB and resulted in its immediate removal in the case of all of the used concentrations (10, 15, and 20 ppm). Also, it has to be noticed that because of the electrophilic nature of MB and the nucleophilic nature of BH_4^- ions, these ions get adsorbed on the rGO-AuNP surface. Subsequently, rGO-AuNPs accept electrons from BH_4^- to form BH_3^{3-} and transmit them to the adsorbed dye molecules rapidly.[74] In addition, the OH groups over the surface of rGO-AuNPs were suggested to effectively interact with cationic MB molecules *via* electrostatic interactions and hydrogen bonding, which improved the removal of the MB dye.[75]

2.9. Antimicrobial Study of AuNPs and rGO-AuNPs. The potentiality of using green synthesized AuNPs and rGO-AuNPs as antibacterial agents against Gram-negative and Gram-positive bacteria at a concentration of 100 $mg{\cdot}mL^{-1}$ was determined using the zone of inhibition as shown in Figure 8.

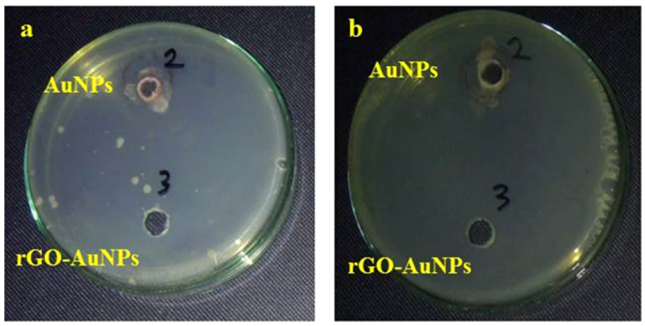

Figure 8. Antibacterial effect of AuNPs and rGO-AuNPs against (a) *E. coli* and (b) *K. pneumonia*.

The bacterial strains used in the current study are *E. coli* and *Klebsiella pneumonia* (Gram-negative bacteria) and also *Bacillus subtilis* and *S. aureus* (Mrsa) (Gram-positive bacteria). Our results revealed that there was no growth detected at all for *E. coli* and *K. pneumonia* in the case of rGO-AuNPs, indicating that rGO-AuNPs were highly efficient against Gram-negative bacteria. However, AuNPs did not show any activity against Gram-negative bacteria. Also, it has to be observed that both nanomaterials did not exhibit any activity against Gram-positive bacteria. The antibacterial activity of rGO-AuNPs is suggested to be related to changing the shape of the cell membrane and inhibiting normal budding owing to a loss of membrane integrity, leading to an increase in the formation of reactive oxygen species (ROS), oxidative stress, a disorder with DNA replication, and finally apoptosis as mentioned in earlier studies.[84,85] Therefore, the acquired data revealed that the rGO-AuNP nanocomposite is a potential antibacterial that has high efficacy against Gram-negative bacteria at a high concentration (2×10^8 CFU/mL). A plausible reason behind such a superior antibacterial activity for rGO-AuNPs synthesized from *P. salicifolia* is that the extract of *P. salicifolia* contains several antioxidant, analgesic, antimicrobial, and antitumor active biochemical ingredients.[86,87] Furthermore, these plants were proven to have many medicinal benefits[50] as they contain phenolic acids, glycosides, terpenoids, and flavonoids. In addition, a comparison between the antibacterial activity of AuNPs, rGO-AuNPs, and other nanomaterials is given in Table 2 to indicate the high antibacterial efficiency of rGO-AuNPs, which is better than various previously reported results.

2.10. Antioxidant Study. As a result of basic and essential metabolic activities, toxic free radicals, including reactive oxygen species (ROS), are usually produced.[95,96] DPPH is characterized as a persistent free radical owing to the molecular delocalization of free electrons across the whole molecule.[97,98] Many antioxidants are efficient in DPPH removal including metal nanoparticles, metal oxides, and graphene nanostructures.[99,100]

In the current study, the scavenging % of DPPH increased steadily from 5.8% to approximately 32.11% when the concentration of rGO-AuNPs increased from 12.5 to 50 μg/mL (Figure 9). This percentage was considered promising, and it is concomitant with other research works. Furthermore, the antioxidant efficiency of rGO-AuNPs could be accredited to the antioxidant potentiality of the *P. salicifolia* aqueous extract.[101] Vitamin C, which is used as a reference, achieved 14.25, 32.05, and 48.7% of DPPH removal at concentrations of 12.5, 25, and 50 μg/mL (Figure 9), respectively, which are higher than that of rGO-AuNPs. All in all, the current results confirmed the good antioxidant capability of the rGO-AuNP nanocomposite against DPPH and its promising application in the scavenging of other free radicals in further studies. Additionally, it has to be mentioned that the antioxidant efficiency of rGO-AuNPs is better than that of AuNPs that we synthesized using the same plant extract in a recent study[101] as the efficiency of AuNPs was 57.7% but at a much higher concentration (300 μg/mL). Furthermore, a comparison between the antioxidant efficiency of rGO-AuNPs and other nanomaterials is presented in Table 3 to indicate the good antioxidant efficiency of rGO-AuNPs, which is comparable to other previously reported results.

3. CONCLUSIONS

According to the aforementioned findings, the following conclusions can be drawn. The *P. salicifolia* aqueous leaf extract was successfully utilized for the synthesis of a rGO-AuNP nanocomposite for the first time according to the available literature. Raman analysis proved that the phytosynthesized rGO was composed of a few sheets as well as demonstrated the high quality of the rGO-AuNPs synthesized using the plant extract with a low defect ratio. AuNPs decorating the rGO surface were shown to be mostly spherical with an average particle size of 15−20 nm. However, other shapes were sporadically recorded including triangles, rods, and rhomboids. Results demonstrated the higher efficiency of rGO-AuNPs in all of the tested applications compared to pristine AuNPs. The catalytic degradation efficiency of rGO-AuNPs reached almost 100% against all of the MB concentrations, while the recorded degradation percentage of AuNPs was 24% at the highest concentration (20 ppm). rGO-AuNPs acquired a potent antibacterial effect against *E. coli* and *K. pneumonia*, whereas AuNPs did not exhibit any effect. A prominent antioxidant efficacy of rGO-AuNPs was also evident. These findings confirmed the higher efficacy of rGO-AuNPs compared to AuNPs phytosynthesized using the same plant extract in the applications studied in this work.

4. MATERIALS AND METHODS

4.1. Chemicals and Reagents. All reagents used without further purification in this study including sodium nitrate ($NaNO_3$), potassium permanganate ($KMnO_4$), hydrogen peroxide (H_2O_2), sulfuric acid (H_2SO_4), sodium borohydride

https://doi.org/10.1021/acsomega.1c05596
ACS Omega 2021, 6, 34954−34966

Table 2. Comparison between the Antimicrobial Efficiency of AuNPs and rGO-AuNPs Synthesized in the Current Study and Other Nanomaterials Mentioned in Other Studies

sample	sample concentration ($mg{\cdot}mL^{-1}$)	bacterial strain	zone of inhibition (mm)	refs
reduced graphene oxide (rGO)	100	*E. coli*	18	88
		S. aureus	23	
graphene oxide (GO)		*E. coli*	resistant	
		S. aureus	resistant	
palladium-decorated reduced graphene oxide/zinc oxide nanocomposite (Pd-RGO-ZnO)		*K. pneumonia*	11	89
		P. aeruginosa	10	
reduced graphene oxide (rGO)		*E. coli*	11	90
silver-reduced graphene oxide nanocomposite (Ag-rGO)	100	*S. aureus*	8	91
		B. subtilis	9	
		E. coli	18	
reduced graphene oxide–zinc oxide nanocomposite (RGO-ZnO)	200	*K. pneumonia*	14	92
		P. aeruginosa	14.5	
gold-reduced graphene oxide nanocomposite (Au-rGO)	150	*K. pneumonia*	23.4	93
		P. aeruginosa	24.4	
		S. aureus	21.4	
graphene oxide (GO)	100	*B. subtilis*	9	94
		E. coli	8	
		P. aeruginosa	6	
reduced graphene oxide (rGO)		*B. subtilis*	18	
		E. coli	14	
		P. aeruginosa	7.5	
gold nanoparticles (AuNPs)	100	*E. coli*	resistant	the current work
		K. pneumonia		
		S. aureus		
		B. subtilis		
reduced graphene oxide–gold nanocomposite (rGO-AuNPs)		*E. coli*	no growth (sensitive)	
		K. pneumonia		
		S. aureus	resistant	
		B. subtilis		

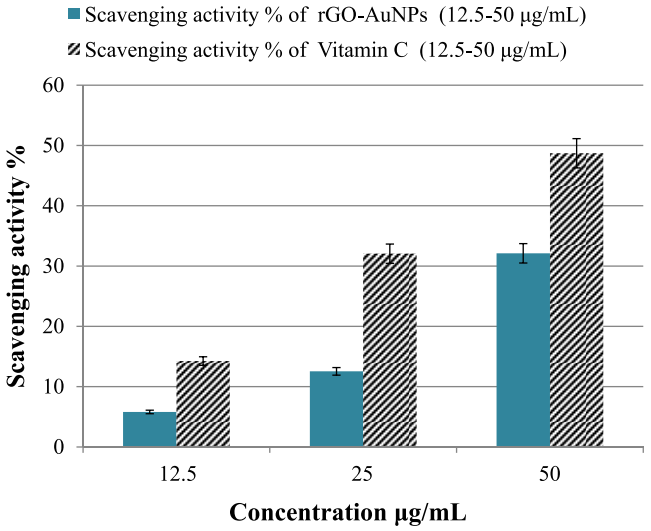

Figure 9. Antioxidant efficiency of rGO-AuNPs and vitamin C (reference) against DPPH.

($NaBH_4$), gold tetrachloroaurate solution ($HAuCl_4{\cdot}3H_2O$), sodium hydroxide (NaOH), sodium borohydride ($NaBH_4$), and methylene blue (MB) were purchased from Merck.

4.2. Collection of Plant Specimens and Preparation of Extracts. Representative samples of *P. salicifolia* leaves were collected from the Nile delta in northern Egypt. Leaves were rinsed with deionized water (DW) several times to remove impurities and debris. Then, leaves were shredded and left to dry in open air, followed by overnight drying at 60 °C till a constant weight is reached. Afterward, dry leaves were ground in a stainless steel mixer to obtain a fine powder. Five grams of this powder was mixed with 100 mL of DW, stirred, and heated at 85 °C for approximately 15 min, and eventually, it was filtered and the filtrate extract was stored in a glass beaker at 4.0 °C for further use.

4.3. Phytosynthesis of AuNPs and rGO-AuNPs. For AuNP synthesis, 1 mL of the obtained leaf extract was mixed with 1 mL of $HAuCl_4{\cdot}3H_2O$ (0.011 M); then, an instantaneous color change was detected from golden yellow to violet at room temperature. The purification step was conducted via centrifugation of the AuNP colloidal solution and then collecting the precipitated pellets and washing them using DW. This step was repeated three times to purify the AuNPs when synthesized or generated. Then, the formed colloidal solution was stored at 4.0 °C for further use. For rGO-AuNP synthesis, 1 mL of the gold ion solution was mixed with the graphene oxide (GO) solution, which was prepared via the modified Hummers method,[107] with a concentration of 0.1 $mg{\cdot}mL^{-1}$; next the mixture solution was stirred and heated at 40 °C for 30 min to promote the interaction between gold ions and GO surfaces, and then, 2 mL of the plant extract was

https://doi.org/10.1021/acsomega.1c05596
ACS Omega 2021, 6, 34954−34966

Table 3. Comparison between the Antioxidant Efficiency of rGO-AuNPs Synthesized in the Current Study and Other Metal Nanomaterials Prepared in Other Studies

antioxidant	concentration (μg/mL)	scavenging percentage (%)	refs
reduced graphene oxide (rGO)	160	25	102
graphene oxide (GO)	400	40	103
zinc oxide−reduced graphene oxide nanocomposite (ZnO-rGO)		22	
reduced graphene oxide−Zinc oxide nanocomposite (RGO-ZnO)	200	45	92
graphene oxide (GO)	100	55	94
reduced graphene oxide (rGO)		80	
reduced graphene oxide quantum dots (rGOQDs)	160	80	104
graphene oxide (GO)	200	20	105
reduced graphene oxide (rGO)		30	
graphene oxide (GO)	750	25	37
reduced graphene oxide (rGO)		60	
graphene oxide (GO)	200	60	91
silver-reduced graphene oxide nanocomposite (Ag-rGO)		90	
graphene oxide (GO)	100	55	106
reduced graphene oxide (rGO)		80	
gold nanoparticles (AuNPs)	300	57.7	36
reduced graphene oxide (rGO-AuNPs)	50	32.11	the current work

added under stirring and heating at 70 °C for 6 h. Furthermore, a black precipitate was noticed, and the solution was centrifuged at 5000 rpm and washed many times with DW until neutralization. Eventually, the pellets were dried overnight in an oven at 50 °C, and then they were stored for further use.

4.4. Characterization Techniques. UV−Visible spectroscopy measurements were conducted *via* a double-beam spectrophotometer (T70/T80 series UV/Vis spectrophotometer, PG instruments Ltd, U.K.), in the scanning range 200−800 nm. TEM measurements were performed on a JEOL, JEM-2100F, Japan, operated at an accelerating voltage of 200 kV. FTIR measurements were conducted on a JASCO spectrometer in the range 4000−600 cm^{-1}. ζ potential was examined in a ζ potential analyzer (Zetasizer Nano ZS Malvern). XRD was conducted on an X-ray diffractometer (X'Pert PRO, The Netherlands) operated at a voltage of 45 kV and a current of 40 mA with Cu Kα1 radiation (λ = 1.54056 Å) in the 2θ range from 20 to 80°. Energy-dispersive X-ray spectroscopy (EDX) was performed by a JEOL model JSM-IT100. Raman spectroscopy was performed on the dried sample at room temperature using a SENTERRA Raman spectrometer, Bruker, Germany, with a 514.5 nm excitation wavelength to determine the extent of graphitic disorder within the prepared material.

4.5. Catalytic Degradation of Methylene Blue (MB). Briefly, 0.1 mL of AuNPs and rGO-AuNPs were added separately to 10 mL of various aqueous solutions of MB with concentrations ranging from 10 to 20 ppm (10, 15, and 20 ppm). Then, 0.1 mL of freshly prepared aqueous $NaBH_4$ solution (0.058 M) was added to these solutions. Progress of the reaction was monitored by recording the time-dependent UV−vis absorption spectra of these mixtures at 664 nm in a quartz cuvette (path length 1 cm) using UV−vis spectroscopy (T70/T80 series UV/vis spectrophotometer, PG instruments Ltd, U.K.). Control experiments were conducted under the same experimental conditions yet without AuNPs, rGO-AuNPs, or $NaBH_4$. Scanning was performed in the range 200−800 nm at ambient room temperature (25 °C), and the efficacy was measured by the following equation[80,108]

$$\text{degradation percentage \% of MB} = \frac{A_0 - A}{A_0} \times 100 \quad (1)$$

where A_0 represents the initial absorbance and A refers to the final absorbance.

4.6. Antimicrobial Test. *4.6.1. Inoculum Preparation.* The stock culture of reference strains (in glycerol broth) was subcultured onto tryptic soy agar plates. After overnight incubation, the tops of 3−5 colonies of pure culture of the organism to be tested (*E. coli* (ATCC 8739), *K. pneumonia* (ATCC 1388), *B. subtilis* (ATCC 6633), and *S. aureus* (Mrsa) (ATCC 25923)) were touched with a loop and suspended in a sterile test tube containing 2 mL of saline. Turbidity of the suspended colonies was compared with the 0.5 McFarland turbidity standard equivalent to 2 × 10^8 CFU/mL, and the density of the organism suspension was adjusted by adding more bacteria or more sterile saline.

4.6.2. Preparation of Seeded Agar. Muller Hinton agar was weighed and dissolved in distilled water and then sterilized by autoclaving after being divided into 25 mL portions into six separate flasks. Flasks were left to cool to 50 °C, and then tested reference strains (1%) were added on sterile Muller Hinton agar. Flasks were shaken and poured onto sterile Petri dishes and left to solidify. With a sterile cork borer, three wells (each 8 mm diameter) were made in each seeded agar plate.

4.6.3. Placing of Tested Materials (AuNPs and rGO-AuNPs). The panel of the selected material to be evaluated was placed on the inoculated plates using a sterile automatic pipette directly onto its specific well after sterilization by filtration; the plates were put in the refrigerator overnight to allow the diffusion of tested materials.

4.6.4. Incubation. Plates were incubated at 35 ± 2 °C for 24 h.

4.6.5. Reading Results. All measurements were made with the unaided eye while viewing the back of the Petri dish a few inches above a nonreflecting background and illuminated with reflected light.

4.7. Antioxidant Activity of rGO-AuNPs (DPPH Assay). The free radical scavenging activity was examined via the DPPH (2,2-diphenyl-1-picrylhydrazyl) assay to measure the antioxidant efficiency of both AuNP and rGO-AuNP samples. The assay was conducted in triplicate. Briefly, 1 mL of each sample was mixed with 1 mL of DPPH (0.2 mM) along with a control sample. Solutions were mixed for 3 min under dark conditions at room temperature. Then, after 20 min, the radical's concentration was measured by the reduction in absorbance % of the mixture at 517 nm wavelength. The absorbance change was measured at 517 nm. Vitamin C (ascorbic acid) was employed as a positive control. The activity was measured by the following equation[109,110]

$$\text{radical scavenging activity} = \frac{(\text{control absorbance} - \text{sample absorbance})}{\text{control absorbance}} \times 100 \quad (2)$$

https://doi.org/10.1021/acsomega.1c05596
ACS Omega 2021, 6, 34954−34966

where control absorbance is the absorbance in the absence of antioxidants and sample absorbance is the absorbance in the presence of antioxidants (AuNPs, rGO-AuNPs, or vitamin C) at 517 nm.

4.8. Statistical Analysis. All experiments were conducted in triplicates ($n = 3$), while the gained data were presented as a mean value corrected by the standard deviation (±SD).

■ ASSOCIATED CONTENT

Supporting Information

The Supporting Information is available free of charge at https://pubs.acs.org/doi/10.1021/acsomega.1c05596.

> ζ potential of GO and rGO-AuNPs; EDX spectrum of rGO-AuNPs; Raman spectra of GO and rGO-AuNPs; efficiency of *P. salicifolia* extract in MB (15 ppm) catalytic degradation; reusability of rGO-AuNPs in MB catalytic degradation and removal percentage with the number of cycles (PDF)

■ AUTHOR INFORMATION

Corresponding Author

Mohamed Hosny − *Green Technology Group, Environmental Sciences Department, Faculty of Science, Alexandria University, 21511 Alexandria, Egypt;* orcid.org/0000-0001-6824-5459; Email: MohamedHosny@alexu.edu.eg, mohamedhosnymetal09@gmail.com

Authors

Nourhan El-Maghrabi − *Green Technology Group, Environmental Sciences Department, Faculty of Science, Alexandria University, 21511 Alexandria, Egypt*

Ola M. El-Borady − *Institute of Nanoscience and Nanotechnology, Kafrelsheikh University, Kafrelsheikh 33516, Egypt;* orcid.org/0000-0002-4168-5697

Manal Fawzy − *Green Technology Group, Environmental Sciences Department, Faculty of Science, Alexandria University, 21511 Alexandria, Egypt; National Egyptian Biotechnology Experts Network, National Egyptian Academy for Scientific Research and Technology, Cairo 33516, Egypt;* orcid.org/0000-0002-9401-9049

Complete contact information is available at: https://pubs.acs.org/10.1021/acsomega.1c05596

Author Contributions

N.E.-M. was responsible for carrying out the experimental work of the characterization part, investigation, data analysis, and writing of the original draft. M.F. was responsible for conceptualization, funding acquisition, project administration, supervision, validation, and reviewing of the final manuscript. M.H. was responsible for the investigation, formal analysis, methodology, data curation and visualization, and writing of the original draft. O.M.E.-B. was responsible for the supervision of the experimental work, data curation, and visualization.

Notes

The authors declare no competing financial interest.

■ ACKNOWLEDGMENTS

This work was supported by SMARTWATIR, ERANETMED-3-227 project, Academy of Scientific Research and Technology & UNESCO Young Scientist Research Grant 2020, and Egyptian National MAB Committee for UNESCO. This support was used in purchasing of chemicals.

■ REFERENCES

(1) Nowack, B.; Bucheli, T. D. Occurrence, behavior and effects of nanoparticles in the environment. *Environ. Pollut.* **2007**, *150*, 5−22.

(2) Takai-Yamashita, C.; Mabuchi, Y.; Senna, M.; Fuji, M.; Ohya, Y.; Yamagata, Y. Microstructure and surface activity of mechanically-dispersed cellulose nanofiber aqueous sol. *Cellulose* **2021**, *28*, 775−785.

(3) Nakashima, Y.; Takai, C.; Razavi-Khosroshahi, H.; Fuji, M. Effects of cations on the size and silica shell microstructure of hollow silica nanoparticles prepared using PAA/cation/NH4OH template. *Colloids Surf., A* **2020**, *593*, No. 124582.

(4) Hu, R.; Furukawa, T.; Gong, Y.; Chen, L.; Wang, X.; Tian, X.; Nagatsu, M. Tailoring of Cu@ graphitic carbon nanostructures enables the selective detection of copper ions and highly efficient catalysis of organic pollutants. *Adv. Mater. Interfaces* **2018**, *5*, No. 1800551.

(5) Sondhi, P.; Maruf, M. H. U.; Stine, K. J. Nanomaterials for biosensing lipopolysaccharide. *Biosensors* **2020**, *10*, No. 2.

(6) Gazzi, A.; Fusco, L.; Orecchioni, M.; Ferrari, S.; Franzoni, G.; Yan, J. S.; Rieckher, M.; Peng, G.; Lucherelli, M. A.; Vacchi, I. A.; et al. Graphene, other carbon nanomaterials and the immune system: toward nanoimmunity-by-design. *J. Phys. Mater.* **2020**, *3*, No. 034009.

(7) Liu, S.; Tian, J.; Wang, L.; Luo, Y.; Sun, X. One-pot synthesis of CuO nanoflower-decorated reduced graphene oxide and its application to photocatalytic degradation of dyes. *Catal. Sci. Technol.* **2012**, *2*, 339−344.

(8) Allen, M. J.; Tung, V. C.; Kaner, R. B. Honeycomb carbon: a review of graphene. *Chem. Rev.* **2010**, *110*, 132−145.

(9) Liu, S.; Tian, J.; Wang, L.; Zhang, Y.; Luo, Y.; Asiri, A. M.; Al-Youbi, A. O.; Sun, X. A novel acid-driven, microwave-assisted, one-pot strategy toward rapid production of graphitic N-doped carbon nanoparticles-decorated carbon flakes from N, N-dimethylformamide and their application in removal of dye from water. *RSC Adv.* **2012**, *2*, 4632−4635.

(10) Li, F.; Tao, R.; Cao, B.; Yang, L.; Wang, Z. Manipulating the Light-Matter Interaction of PtS/MoS2 p−n Junctions for High Performance Broadband Photodetection. *Adv. Funct. Mater.* **2021**, *31*, No. 2104367.

(11) Qin, T.; Wang, Z.; Wang, Y.; Besenbacher, F.; Otyepka, M.; Dong, M. Recent Progress in Emerging Two-Dimensional Transition Metal Carbides. *Nano-Micro Lett.* **2021**, *13*, No. 183.

(12) Cui, Q.; Yang, Y.; Li, J.; Teng, F.; Wang, X. Material and device architecture engineering toward high performance two-dimensional (2D) photodetectors. *Crystals* **2017**, *7*, No. 149.

(13) Yin, P. T.; Shah, S.; Chhowalla, M.; Lee, K.-B. Design, synthesis, and characterization of graphene−nanoparticle hybrid materials for bioapplications. *Chem. Rev.* **2015**, *115*, 2483−2531.

(14) Cheng, N.; Tian, J.; Liu, Q.; Ge, C.; Qusti, A. H.; Asiri, A. M.; Al-Youbi, A. O.; Sun, X. Au-nanoparticle-loaded graphitic carbon nitride nanosheets: green photocatalytic synthesis and application toward the degradation of organic pollutants. *ACS Appl. Mater. Interfaces* **2013**, *5*, 6815−6819.

(15) Khalil, I.; Julkapli, N. M.; Yehye, W. A.; Basirun, W. J.; Bhargava, S. K. Graphene−gold nanoparticles hybrid—synthesis, functionalization, and application in a electrochemical and surface-enhanced raman scattering biosensor. *Materials* **2016**, *9*, No. 406.

(16) Tien, H.-W.; Huang, Y.-L.; Yang, S.-Y.; Wang, J.-Y.; Ma, C.-C. M. The production of graphene nanosheets decorated with silver nanoparticles for use in transparent, conductive films. *Carbon* **2011**, *49*, 1550−1560.

(17) Wang, F.-B.; Wang, J.; Shao, L.; Zhao, Y.; Xia, X.-H. Hybrids of gold nanoparticles highly dispersed on graphene for the oxygen reduction reaction. *Electrochem. commun.* **2014**, *38*, 82−85.

(18) Slepička, P.; Slepičková Kasálková, N.; Siegel, J.; Kolská, Z.; Švorčík, V. Methods of gold and silver nanoparticles preparation. *Materials* **2020**, *13*, No. 1.

(19) Singh, P.; Pandit, S.; Mokkapati, V.; Garg, A.; Ravikumar, V.; Mijakovic, I. Gold nanoparticles in diagnostics and therapeutics for human cancer. *Int. J. Mol. Sci.* **2018**, *19*, No. 1979.
(20) Badeggi, U. M.; Ismail, E.; Adeloye, A. O.; Botha, S.; Badmus, J. A.; Marnewick, J. L.; Cupido, C. N.; Hussein, A. A. Green synthesis of gold nanoparticles capped with procyanidins from Leucosidea sericea as potential antidiabetic and antioxidant agents. *Biomolecules* **2020**, *10*, No. 452.
(21) Hameed, S.; Ali Shah, S.; Iqbal, J.; Numan, M.; Muhammad, W.; Junaid, M.; Shah, S.; Khurshid, R.; Umer, F. Cannabis sativa-mediated synthesis of gold nanoparticles and their biomedical properties. *Bioinspired, Biomimetic Nanobiomater.* **2020**, *9*, 95−102.
(22) Guo, Y.; Jiang, N.; Zhang, L.; Yin, M. Green synthesis of gold nanoparticles from Fritillaria cirrhosa and its anti-diabetic activity on Streptozotocin induced rats. *Arabian J. Chem.* **2020**, *13*, 5096−5106.
(23) Rajan, A.; Rajan, A. R.; Philip, D. Elettaria cardamomum seed mediated rapid synthesis of gold nanoparticles and its biological activities. *OpenNano* **2017**, *2*, 1−8.
(24) Vijayakumar, S.; Vaseeharan, B.; Malaikozhundan, B.; Gopi, N.; Ekambaram, P.; Pachaiappan, R.; Velusamy, P.; Murugan, K.; Benelli, G.; Kumar, R. S.; et al. Therapeutic effects of gold nanoparticles synthesized using Musa paradisiaca peel extract against multiple antibiotic resistant Enterococcus faecalis biofilms and human lung cancer cells (A549). *Microb. Pathog.* **2017**, *102*, 173−183.
(25) Hamelian, M.; Hemmati, S.; Varmira, K.; Veisi, H. Green synthesis, antibacterial, antioxidant and cytotoxic effect of gold nanoparticles using Pistacia Atlantica extract. *J. Taiwan Inst. Chem. Eng.* **2018**, *93*, 21−30.
(26) Aljabali, A. A.; Akkam, Y.; Al Zoubi, M. S.; Al-Batayneh, K. M.; Al-Trad, B.; Abo Alrob, O.; Alkilany, A. M.; Benamara, M.; Evans, D. J. Synthesis of gold nanoparticles using leaf extract of Ziziphus zizyphus and their antimicrobial activity. *Nanomaterials* **2018**, *8*, No. 174.
(27) El-Monaem, E. M. A.; El-Latif, M. M. A.; Eltaweil, A. S.; El-Subruiti, G. M. Cobalt Nanoparticles Supported on Reduced Amine-Functionalized Graphene Oxide for Catalytic Reduction of Nitroanilines and Organic Dyes. *Nano* **2021**, *16*, No. 2150039.
(28) Eltaweil, A. S.; El-Tawil, A. M.; Abd El-Monaem, E. M.; El-Subruiti, G. M. Zero valent iron nanoparticle-loaded nanobentonite intercalated carboxymethyl chitosan for efficient removal of both anionic and cationic dyes. *ACS Omega* **2021**, *6*, 6348−6360.
(29) Iyer, J. K.; Dickey, A.; Rouhani, P.; Kaul, A.; Govindaraju, N.; Singh, R. N.; Kaul, R. Nanodiamonds facilitate killing of intracellular uropathogenic *E. coli* in an in vitro model of urinary tract infection pathogenesis. *PLoS One* **2018**, *13*, No. e0191020.
(30) Carezzano, M. E.; Sotelo, J. P.; Primo, E.; Reinoso, E. B.; Paletti Rovey, M. F.; Demo, M. S.; Giordano, W. F.; Oliva, M. dlM. Inhibitory effect of Thymus vulgaris and Origanum vulgare essential oils on virulence factors of phytopathogenic Pseudomonas syringae strains. *Plant Biol.* **2017**, *19*, 599−607.
(31) Navidinia, M.; Karimi, A.; Rahbar, M.; Fallah, F.; Ahsani, R. R.; Malekan, M. A.; Jahromi, M. H.; GholineJad, Z. Study prevalence of verotoxigenic *E. coli* isolated from urinary tract infections (UTIs) in an Iranian children hospital. *Open Microbiol. J.* **2012**, *6*, 1.
(32) Zasowski, E. J.; Trinh, T. D.; Claeys, K. C.; Casapao, A. M.; Sabagha, N.; Lagnf, A. M.; Klinker, K. P.; Davis, S. L.; Rybak, M. J. Multicenter observational study of ceftaroline fosamil for methicillin-resistant *Staphylococcus aureus* bloodstream infections. *Antimicrob. Agents Chemother.* **2017**, *61*, e02015−e02016.
(33) Allen, H. K.; Donato, J.; Wang, H. H.; Cloud-Hansen, K. A.; Davies, J.; Handelsman, J. Call of the wild: antibiotic resistance genes in natural environments. *Nat. Rev. Microbiol.* **2010**, *8*, 251−259.
(34) Sathiyaraj, G.; Vinosha, M.; Sangeetha, D.; Manikandakrishnan, M.; Palanisamy, S.; Sonaimuthu, M.; Manikandan, R.; You, S.; Prabhu, N. M. Bio-directed synthesis of Pt-nanoparticles from aqueous extract of red algae Halymenia dilatata and their biomedical applications. *Colloids Surf., A* **2021**, *618*, No. 126434.
(35) Eltaweil, A. S.; Fawzy, M.; Hosny, M.; Abd El-Monaem, E. M.; Tamer, T. M.; Omer, A. M. Green synthesis of platinum nanoparticles using Atriplex halimus leaves for potential antimicrobial, antioxidant, and catalytic applications. *Arab. J. Chem.* **2021**, No. 103517.
(36) Hosny, M.; Fawzy, M. Instantaneous phytosynthesis of gold nanoparticles via *Persicaria salicifolia* leaf extract, and their medical applications. *Adv Powder Technol.* **2021**, *32*, 2891−2904.
(37) Al-Ani, L. A.; Yehye, W. A.; Kadir, F. A.; Hashim, N. M.; AlSaadi, M. A.; Julkapli, N. M.; Hsiao, V. K. Hybrid nanocomposite curcumin-capped gold nanoparticle-reduced graphene oxide: Anti-oxidant potency and selective cancer cytotoxicity. *PLoS One* **2019**, *14*, No. e0216725.
(38) Youssef, A. M. M.; El-Swaify, Z. A. S. Anti-Tumour Effect of two Persicaria Species Seeds on Colon and Prostate Cancers. *Biomed. Pharmacol. J.* **2018**, *11*, 635−644.
(39) Salem, H.; Elhela, A. A.; Abdelhady, N. M. Utility of silver nanoparticles for the analysis of diosmin and rutin in *Persicaria salicifolia* extract, authentic and pharmaceutical dosage forms monitored with their haemostatic activity. *Afr. J. Pharm. Pharmacol.* **2018**, *12*, 248−262.
(40) Brewer, M. Natural antioxidants: sources, compounds, mechanisms of action, and potential applications. *Compr. Rev. Food Sci. Food Saf.* **2011**, *10*, 221−247.
(41) Oh, M.-M.; Carey, E. E.; Rajashekar, C. Environmental stresses induce health-promoting phytochemicals in lettuce. *Plant Physiol. Biochem.* **2009**, *47*, 578−583.
(42) Chen, X.; Su, B.; Wu, G.; Yang, C. J.; Zhuang, Z.; Wang, X.; Chen, X. Platinum nanoflowers supported on graphene oxide nanosheets: their green synthesis, growth mechanism, and advanced electrocatalytic properties for methanol oxidation. *J. Mater. Chem.* **2012**, *22*, 11284−11289.
(43) Ding, Y.; Zhang, P.; Zhuo, Q.; Ren, H.; Yang, Z.; Jiang, Y. A green approach to the synthesis of reduced graphene oxide nanosheets under UV irradiation. *Nanotechnology* **2011**, *22*, No. 215601.
(44) Tabrizi, M. A.; Varkani, J. N. Green synthesis of reduced graphene oxide decorated with gold nanoparticles and its glucose sensing application. *Sens. Actuators, B* **2014**, *202*, 475−482.
(45) Amarnath, K.; Mathew, N. L.; Nellore, J.; Siddarth, C. R.; Kumar, J. Facile synthesis of biocompatible gold nanoparticles from Vites vinefera and its cellular internalization against HBL-100 cells. *Cancer Nanotechnol.* **2011**, *2*, 121−132.
(46) Maddinedi, S. B.; Mandal, B. K.; Vankayala, R.; Kalluru, P.; Pamanji, S. R. Bioinspired reduced graphene oxide nanosheets using Terminalia chebula seeds extract. *Spectrochim. Acta, Part A* **2015**, *145*, 117−124.
(47) Lee, G.; Kim, B. S. Biological reduction of graphene oxide using plant leaf extracts. *Biotechnol. Prog.* **2014**, *30*, 463−469.
(48) Li, X.; Zhao, Y.; Wu, W.; Chen, J.; Chu, G.; Zou, H. Synthesis and characterizations of graphene−copper nanocomposites and their antifriction application. *J. Ind. Eng. Chem.* **2014**, *20*, 2043−2049.
(49) El-Anwar, R.; Ibrahim, A.; Abo El-Seoud, K.; Kabbask, A. Phytochemical and biological studies on *Persicaria salicifolia* Brouss. Ex Willd growing in Egypt. *Int. Res. J. Pharm.* **2016**, *7*, 4−12.
(50) Hussein, S.; Usama, E.-M.; Tantawy, M.; Kawashty, S.; Saleh, N. Phenolics of selected species of Persicaria and Polygonum (Polygonaceae) in Egypt. *Arab. J. Chem.* **2017**, *10*, 76−81.
(51) Mahata, S.; Sahu, A.; Shukla, P.; Rai, A.; Singh, M.; Rai, V. K. The novel and efficient reduction of graphene oxide using Ocimum sanctum L. leaf extract as an alternative renewable bio-resource. *New J. Chem.* **2018**, *42*, 19945−19952.
(52) Khan, M.; Al-Marri, A. H.; Khan, M.; Shaik, M. R.; Mohri, N.; Adil, S. F.; Kuniyil, M.; Alkhathlan, H. Z.; Al-Warthan, A.; Tremel, W.; et al. Green approach for the effective reduction of graphene oxide using Salvadora persica L. root (Miswak) extract. *Nanoscale Res. Lett.* **2015**, *10*, 1−9.
(53) Zubar, T.; Fedosyuk, V.; Tishkevich, D.; Kanafyev, O.; Astapovich, K.; Kozlovskiy, A.; Zdorovets, M.; Vinnik, D.; Gudkova, S.; Kaniukov, E.; et al. The effect of heat treatment on the microstructure and mechanical properties of 2D nanostructured Au/NiFe system. *Nanomaterials* **2020**, *10*, 1077.

https://doi.org/10.1021/acsomega.1c05596
ACS Omega 2021, 6, 34954−34966

(54) Trukhanov, A. V.; Darwish, K.; Salem, M.; Hemeda, O.; Ati, M. A.; Darwish, M.; Kaniukov, E.; Podgornaya, S.; Turchenko, V.; Tishkevich, D.; et al. Impact of the heat treatment conditions on crystal structure, morphology and magnetic properties evolution in BaM nanohexaferrites. *J. Alloys Compd.* **2021**, *866*, No. 158961.
(55) Mhamane, D.; Ramadan, W.; Fawzy, M.; Rana, A.; Dubey, M.; Rode, C.; Lefez, B.; Hannoyer, B.; Ogale, S. From graphite oxide to highly water dispersible functionalized graphene by single step plant extract-induced deoxygenation. *Green Chem.* **2011**, *13*, 1990−1996.
(56) Liu, D.; Bian, Q.; Li, Y.; Wang, Y.; Xiang, A.; Tian, H. Effect of oxidation degrees of graphene oxide on the structure and properties of poly (vinyl alcohol) composite films. *Compos. Sci. Technol.* **2016**, *129*, 146−152.
(57) Al-Sherbini, A.-S.; Bakr, M.; Ghoneim, I.; Saad, M. Exfoliation of graphene sheets via high energy wet milling of graphite in 2-ethylhexanol and kerosene. *J. Adv. Res* **2017**, *8*, 209−215.
(58) Stobinski, L.; Lesiak, B.; Malolepszy, A.; Mazurkiewicz, M.; Mierzwa, B.; Zemek, J.; Jiricek, P.; Bieloshapka, I. Graphene oxide and reduced graphene oxide studied by the XRD, TEM and electron spectroscopy methods. *J. Electron. Spectros. Relat. Phenomena* **2014**, *195*, 145−154.
(59) Jin, X.; Li, N.; Weng, X.; Li, C.; Chen, Z. Green reduction of graphene oxide using eucalyptus leaf extract and its application to remove dye. *Chemosphere* **2018**, *208*, 417−424.
(60) Karthik, R.; Govindasamy, M.; Chen, S.-M.; Mani, V.; Lou, B.-S.; Devasenathipathy, R.; Hou, Y.-S.; Elangovan, A. Green synthesized gold nanoparticles decorated graphene oxide for sensitive determination of chloramphenicol in milk, powdered milk, honey and eye drops. *J. Colloid Interface Sci.* **2016**, *475*, 46−56.
(61) Kadiyala, N. K.; Mandal, B. K.; Ranjan, S.; Dasgupta, N. Bioinspired gold nanoparticles decorated reduced graphene oxide nanocomposite using Syzygium cumini seed extract: Evaluation of its biological applications. *Mater. Sci. Eng., C* **2018**, *93*, 191−205.
(62) Dong, X.; Huang, W.; Chen, P. In situ synthesis of reduced graphene oxide and gold nanocomposites for nanoelectronics and biosensing. *Nanoscale Res Lett.* **2011**, *6*, No. 60.
(63) Konkena, B.; Vasudevan, S. Understanding aqueous dispersibility of graphene oxide and reduced graphene oxide through p K a measurements. *J. Phys. Chem. Lett.* **2012**, *3*, 867−872.
(64) Roy, I.; Bhattacharyya, A.; Sarkar, G.; Saha, N. R.; Rana, D.; Ghosh, P. P.; Palit, M.; Das, A. R.; Chattopadhyay, D. In situ synthesis of a reduced graphene oxide/cuprous oxide nanocomposite: a reusable catalyst. *RSC Adv.* **2014**, *4*, 52044−52052.
(65) Zhu, X.; Xu, X.; Liu, F.; Jin, J.; Liu, L.; Zhi, Y.; Chen, Z.-w.; Zhou, Z.-s.; Yu, J. Green synthesis of graphene nanosheets and their in vitro cytotoxicity against human prostate cancer (DU 145) cell lines. *Nanomater. Nanotechnol.* **2017**, *7*, No. 1847980417702794.
(66) Salunke, B. K.; Kim, B. S. Facile synthesis of graphene using a biological method. *RSC Adv.* **2016**, *6*, 17158−17162.
(67) Wang, H.; Wang, Y.; Cao, X.; Feng, M.; Lan, G. Vibrational properties of graphene and graphene layers. *J. Raman Spectrosc.* **2009**, *40*, 1791−1796.
(68) Hou, D.; Liu, Q.; Wang, X.; Quan, Y.; Qiao, Z.; Yu, L.; Ding, S. Facile synthesis of graphene via reduction of graphene oxide by artemisinin in ethanol. *J. Materiomics* **2018**, *4*, 256−265.
(69) Khojasteh, H.; Safajou, H.; Mortazavi-Derazkola, S.; Salavati-Niasari, M.; Heydaryan, K.; Yazdani, M. Economic procedure for facile and eco-friendly reduction of graphene oxide by plant extracts; a comparison and property investigation. *J. Clean. Prod.* **2019**, *229*, 1139−1147.
(70) Vázquez-Sánchez, P.; Rodríguez-Escudero, M.; Burgos, F.; Llorente, I.; Caballero-Calero, O.; González, M. M.; Fernández, R.; García-Alonso, M. Synthesis of Cu/rGO composites by chemical and thermal reduction of graphene oxide. *J. Alloys Compd.* **2019**, *800*, 379−391.
(71) Chabot, V.; Kim, B.; Sloper, B.; Tzoganakis, C.; Yu, A. High yield production and purification of few layer graphene by Gum Arabic assisted physical sonication. *Sci. Rep.* **2013**, *3*, No. 1378.
(72) Wu, Q.; Zhang, H.; Zhou, L.; Bao, C.; Zhu, H.; Zhang, Y. Synthesis and application of rGO/CoFe2O4 composite for catalytic degradation of methylene blue on heterogeneous Fenton-like oxidation. *J. Taiwan Inst. Chem. Eng.* **2016**, *67*, 484−494.
(73) Chen, S.; Chen, D.; Wang, W.; Quan, H.; Luo, X.; Guo, L. rGO-stabilized MnO/N-doped carbon nanofibers for efficient removal of Pb (II) ion and catalytic degradation of methylene blue. *J. Mater. Sci.* **2017**, *52*, 5117−5132.
(74) Ucar, A.; Findik, M.; Gubbuk, I. H.; Kocak, N.; Bingol, H. Catalytic degradation of organic dye using reduced graphene oxide−polyoxometalate nanocomposite. *Mater. Chem. Phys.* **2017**, *196*, 21−28.
(75) Rani, G. J.; Rajan, M. J.; et al. Reduced graphene oxide/ZnFe2O4 nanocomposite as an efficient catalyst for the photocatalytic degradation of methylene blue dye. *Res. Chem. Intermed.* **2017**, *43*, 2669−2690.
(76) Kar, P.; Sardar, S.; Liu, B.; Sreemany, M.; Lemmens, P.; Ghosh, S.; Pal, S. K. Facile synthesis of reduced graphene oxide−gold nanohybrid for potential use in industrial waste-water treatment. *Sci. Technol. Adv. Mater.* **2016**, *17*, 375−386.
(77) Saleh, R.; Taufik, A. Photo-Fenton degradation of methylene blue in the presence of Au-Fe3O4/graphene composites under UV and visible light at near neutral pH: Effect of coexisting inorganic anion. *Environ. Nanotechnol. Monit. Manag.* **2019**, *11*, No. 100221.
(78) Mahajan, H.; Arumugasamy, S. K.; Panda, A.; Sada, V.; Yoon, M.; Yun, K. Well-Designed Au Nanorod-Doped Cu2O Core−Shell Nanocube-Embedded Reduced Graphene Oxide Composite for Efficient Removal of a Water Pollutant Dye. *ACS Omega* **2020**, *5*, 24799−24810.
(79) Yang, Y.; Ma, Z.; Xu, L.; Wang, H.; Fu, N. Preparation of reduced graphene oxide/meso-TiO2/AuNPs ternary composites and their visible-light-induced photocatalytic degradation n of methylene blue. *Appl. Surf. Sci.* **2016**, *369*, 576−583.
(80) Liu, X.; Huang, L.; Zhang, D.; Yan, T.; Zhang, J.; Shi, L. Light driven fabrication of highly dispersed Mn-Co/RGO and the synergistic effect in catalytic degradation of methylene blue. *Mater. Des.* **2018**, *140*, 286−294.
(81) Sahu, D.; Sahoo, G.; Mohapatra, P.; Swain, S. K. Dual activities of nano silver embedded reduced graphene oxide using clove leaf extracts: Hg2+ sensing and catalytic degradation. *ChemistrySelect* **2019**, *4*, 2593−2602.
(82) Zou, L.; Qu, R.; Gao, H.; Guan, X.; Qi, X.; Liu, C.; Zhang, Z.; Lei, X. MoS2/RGO hybrids prepared by a hydrothermal route as a highly efficient catalytic for sonocatalytic degradation of methylene blue. *Results Phys.* **2019**, *14*, 102458−102468.
(83) Qu, J.; Shi, L.; He, C.; Gao, F.; Li, B.; Zhou, Q.; Hu, H.; Shao, G.; Wang, X.; Qiu, J. Highly efficient synthesis of graphene/MnO2 hybrids and their application for ultrafast oxidative decomposition of methylene blue. *Carbon* **2014**, *66*, 485−492.
(84) Liu, S.; Zeng, T. H.; Hofmann, M.; Burcombe, E.; Wei, J.; Jiang, R.; Kong, J.; Chen, Y. Antibacterial activity of graphite, graphite oxide, graphene oxide, and reduced graphene oxide: membrane and oxidative stress. *ACS Nano* **2011**, *5*, 6971−6980.
(85) Sengupta, I.; Bhattacharya, P.; Talukdar, M.; Neogi, S.; Pal, S. K.; Chakraborty, S. Bactericidal effect of graphene oxide and reduced graphene oxide: Influence of shape of bacteria. *Colloids Interface Sci. Commun.* **2019**, *28*, 60−68.
(86) Khatun, A.; Imam, M. Z.; Rana, M. S. Antinociceptive effect of methanol extract of leaves of Persicaria hydropiper in mice. *BMC Complement Altern.* **2015**, *15*, 1−8.
(87) Uddin, M. S.; Nasrullah, M.; Hossain, M. S.; Rahman, M. M.; Sarwar, M. S.; Amran, M. S.; Sadik, M. G.; Rashid, M.; Asaduzzaman, M. Evaluation of nootropic activity of Persicaria flaccida on cognitive performance, brain antioxidant markers and acetylcholinesterase activity in rats: implication for the management of Alzheimer's disease. *Am. J. Psychiatry.* **2016**, *4*, 26−37.
(88) Vatandost, E.; Saraei, A. G. H.; Chekin, F.; Raeisi, S. N.; Shahidi, S. A. Antioxidant, Antibacterial and Anticancer Performance

https://doi.org/10.1021/acsomega.1c05596
ACS Omega 2021, 6, 34954−34966

of Reduced Graphene Oxide Prepared via Green Tea Extract Assisted Biosynthesis. *ChemistrySelect* **2020**, *5*, 10401−10406.
(89) Rajeswari, R.; Prabu, H. G. Palladium−Decorated reduced graphene oxide/zinc oxide nanocomposite for enhanced antimicrobial, antioxidant and cytotoxicity activities. *Process Biochem.* **2020**, *93*, 36−47.
(90) Joshi, S.; Siddiqui, R.; Sharma, P.; Kumar, R.; Verma, G.; Saini, A. Green synthesis of peptide functionalized reduced graphene oxide (rGO) nano bioconjugate with enhanced antibacterial activity. *Sci. Rep.* **2020**, *10*, No. 9441.
(91) Rajeswari, R.; Prabu, H. G.; Amutha, D. M. One Pot Hydrothermal synthesis characterizations of silver nanoparticles on reduced graphene oxide for its enhanced antibacterial and antioxidant properties. *IOSR J. Appl. Chem.* **2017**, *10*, 64−69.
(92) Rajeswari, R.; Prabu, H. G. Synthesis characterization, antimicrobial, antioxidant, and cytotoxic activities of ZnO nanorods on reduced graphene oxide. *J. Inorg. Organomet. Polym. Mater.* **2018**, *28*, 679−693.
(93) Saikia, I.; Sonowal, S.; Pal, M.; Boruah, P. K.; Das, M. R.; Tamuly, C. Biosynthesis of gold decorated reduced graphene oxide and its biological activities. *Mater. Lett.* **2016**, *178*, 239−242.
(94) Thiyagarajulu, N.; Arumugam, S.; Narayanan, A. L.; Mathivanan, T.; Renuka, R. R. Green Synthesis of Reduced Graphene Nanosheets using Leaf Extract of Tridax procumbens and its Potential In Vitro Biological Activities. *Biointerface Res. Appl. Chem* **2020**, *11*, 9975−9984.
(95) Sen, S.; Chakraborty, R.; Sridhar, C.; Reddy, Y.; De, B. Free radicals, antioxidants, diseases and phytomedicines: current status and future prospect. *Int. J. Pharm. Sci. Rev. Res.* **2010**, *3*, 91−100.
(96) Mittler, R. ROS are good. *Trends Plant Sci.* **2017**, *22*, 11−19.
(97) Kedare, S. B.; Singh, R. Genesis and development of DPPH method of antioxidant assay. *J. Food Sci. Technol.* **2011**, *48*, 412−422.
(98) Thaipong, K.; Boonprakob, U.; Crosby, K.; Cisneros-Zevallos, L.; Byrne, D. H. Comparison of ABTS, DPPH, FRAP, and ORAC assays for estimating antioxidant activity from guava fruit extracts. *J. Food Compost. Anal.* **2006**, *19*, 669−675.
(99) Bhakya, S.; Muthukrishnan, S.; Sukumaran, M.; Muthukumar, M. Biogenic synthesis of silver nanoparticles and their antioxidant and antibacterial activity. *Appl. Nanosci.* **2016**, *6*, 755−766.
(100) Shah, S. T.; A Yehya, W.; Saad, O.; Simarani, K.; Chowdhury, Z.; A Alhadi, A.; Al-Ani, L. A. Surface functionalization of iron oxide nanoparticles with gallic acid as potential antioxidant and antimicrobial agents. *Nanomaterials* **2017**, *7*, No. 306.
(101) Hosny, M.; Fawzy, M. Instantaneous phytosynthesis of gold nanoparticles via *Persicaria salicifolia* leaf extract, and their medical applications. *Adv. Powder Technol.* **2021**, *32*, 2891−2904.
(102) Yang, J.; Huang, Y.; Lv, Y.; Li, S.; Yang, Q.; Li, G. The synergistic mechanism of thermally reduced graphene oxide and antioxidant in improving the thermo-oxidative stability of polypropylene. *Carbon* **2015**, *89*, 340−349.
(103) Baali, N.; Khecha, A.; Bensouici, A.; Speranza, G.; Hamdouni, N. Assessment of antioxidant activity of pure graphene oxide (GO) and ZnO-decorated reduced graphene oxide (rGO) using DPPH radical and H2O2 scavenging assays. *C* **2019**, *5*, 75.
(104) Murugesan, B.; Sonamuthu, J.; Pandiyan, N.; Pandi, B.; Samayanan, S.; Mahalingam, S. Photoluminescent reduced graphene oxide quantum dots from latex of Calotropis gigantea for metal sensing, radical scavenging, cytotoxicity, and bioimaging in Artemia salina: a greener route. *J. Photochem. Photobiol. B: Biol.* **2018**, *178*, 371−379.
(105) Mahmudzadeh, M.; Yari, H.; Ramezanzadeh, B.; Mahdavian, M. Highly potent radical scavenging-anti-oxidant activity of biologically reduced graphene oxide using Nettle extract as a green biogenic amines-based reductants source instead of hazardous hydrazine hydrate. *J. Hazard. Mater.* **2019**, *371*, 609−624.
(106) Thiyagarajulu, N.; Arumugam, S. Green Synthesis of Reduced Graphene oxide Nanosheets Using Leaf Extract of Lantana camara and Its In-Vitro Biological Activities. *J. Cluster Sci.* **2021**, *32*, 559−568.
(107) Chen, J.; Yao, B.; Li, C.; Shi, G. An improved Hummers method for eco-friendly synthesis of graphene oxide. *Carbon* **2013**, *64*, 225−229.
(108) Hosny, M.; Fawzy, M.; El-Borady, O. M.; Mahmoud, A. E. D. Comparative study between Phragmites australis root and rhizome extracts for mediating gold nanoparticles synthesis and their medical and environmental applications. *Adv. Powder Technol.* **2021**, *32*, 2268−2279.
(109) El-Borady, O. M.; Fawzy, M.; Hosny, M. Antioxidant, anticancer and enhanced photocatalytic potentials of gold nanoparticles biosynthesized by common reed leaf extract. *Appl. Nanosci.* **2021**, 1−12.
(110) Hosny, M.; Fawzy, M.; Abdelfatah, A. M.; Fawzy, E. E.; Eltaweil, A. S. Comparative study on the potentialities of two halophytic species in the green synthesis of gold nanoparticles and their anticancer, antioxidant and catalytic efficiencies. *Adv. Powder Technol.* **2021**, *32*, 3220−3233.

https://doi.org/10.1021/acsomega.1c05596
ACS Omega 2021, 6, 34954−34966